NASA/CR–2001–210851

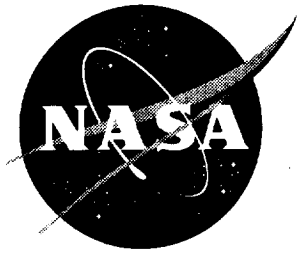

Inviscid Flow Computations of Several Aeroshell Configurations for a '07 Mars Lander

Ramadas K. Prabhu
Lockheed Martin Engineering & Sciences Company, Hampton, Virginia

National Aeronautics and
Space Administration

Langley Research Center
Hampton, Virginia 23681–2199

Prepared for Langley Reseach Center
under contract NAS1-96014

April 2001

Available from the following:

NASA Center for AeroSpace Information (CASI)
7121 Standard Drive
Hanover, MD 21076–1320
(301) 621–0390

National Technical Information Service (NTIS)
5285 Port Royal Road
Springfield, VA 22161–2171
(703) 487–4650

Summary

This report documents the results of an inviscid computational study conducted on several candidate aeroshell configurations for a proposed '07 Mars lander. Eleven different configurations were considered, and the aerodynamic characteristics of each of these were computed for a Mach number of 23.7 at 10, 15, and 20 degrees angles of attack. The unstructured grid software FELISA with the equilibrium Mars gas option was used for these computations. The pitching moment characteristics and the lift-to-drag ratios at trim angle of attack of each of these configurations were examined to make a selection. The criterion for selection was that the configuration should be longitudinally stable, and should trim at an angle of attack where the L/D is -0.25. Based on the present study, two configuration were selected for further study.

Nomenclature

C_A	Axial force coefficient
C_D	Drag coefficient
C_L	Lift coefficient
C_N	Normal force coefficient
C_m	Pitching moment coefficient about the point (0.0, 0.0, -0.8018)
C_p	$(p - p_\infty)/q_\infty$, Pressure coefficient
L/D	C_L / C_D , Lift-to-drag ratio
l_{ref}	Reference length for pitching moment (=3.75 m.)
M_∞	Freestream Mach number
p	Static pressure
p_∞	Freestream static pressure
q_∞	$\rho_\infty U_\infty^2/2$, Freestream dynamic pressure
S_{ref}	Reference area (=11.045 sq. m.)
T_∞	Freestream temperature (K)
U_∞	Freestream velocity (m/s)
x, y, z	Cartesian co-ordinates of a given point; (The origin is at the nose, with the x-axis in the vertical direction, the y-axis in the spanwise direction, and the z-axis in the axial direction pointing into the stream.)
ρ_∞	Freestream density (kg/m^3)
α	Angle of attack, deg.

Introduction

In a effort aimed at arriving at a suitable aeroshell configuration for a proposed '07 Mars lander, an extensive computational study was done. For the purposes of controlling the aeroshell through its entry trajectory it was required that the aeroshell should have a lift-to-drag ratio of -0.25 at the trim angle of attack. The baseline configuration of the aeroshell is symmetric. Hence it would trim only at zero angle of attack and the lift-to-drag at the trim conditions would be zero. In order to make the configuration asymmetric about the pitch axis, tabs, flaps, and bumps of varying sizes and shapes were added to the baseline aeroshell

configuration so that the resulting configuration would trim at a non-zero angle. The pitching moment characteristics and lift-to-drag ratio of each of these configurations were studied.

Unstructured grid technology is known to provide quick and reliable CFD solutions for complex flow problems, particularly for hypersonic flows. Among the widely used unstructured grid software packages are the FELISA [1] and the TetrUSS [2] systems. In the Aerothermodynamics Branch (AB) at NASA Langley Research Center, FELISA inviscid flow solvers have been used extensively for the prediction of flow over complex vehicles. See for example [3] & [4]. FELISA flow solvers, being inviscid, have the obvious limitations; because of the absence of a boundary layer there is no skin friction and no flow separation effects. For lifting bodies the inviscid flow solvers generally yield good normal force and pitching moment results as long as there is no significant flow separation. However, for a blunt body like the proposed aeroshell under hypersonic flow conditions the C_N, C_A, and C_m are primarily due to the pressures over the forebody, and the effects of skin friction are negligible. Further, since the aftbody pressures are small, they contribute little to the vehicle aerodynamics. It is therefore expected that inviscid hypersonic flow computations would give reliable results for the purpose of the present study.

This paper presents the results of an inviscid computational study for several different aeroshell configurations of the '07 Mars lander using the unstructured grid software FELISA with an equilibrium Mars gas option. Only the forebodies of these configurations are simulated, and the aftbodies are ignored. Further, since the aeroshell has a plane of symmetry and only symmetric flow conditions are considered, only one half of the aeroshell is considered in the present study. The present study was done for a Mach number of 23.7 with freestream conditions representing the peak heating point on a preliminary '07 Mars lander trajectory. Computations were done for three angles of attack namely 10, 15, and 20 degrees. The pitching moment characteristics and the lift-to-drag values at the trim angle of attack for each of the configurations were examined. Based on this study, two new configurations were selected for further study.

The FELISA Software

All the computations of the present study were done using the unstructured grid software FELISA. This software package has proved to be a powerful tool for fast inviscid grid generation and flow computations, particularly for Earth atmospheric hypersonic flows (see [3] & [4]). The grid generation part of FELISA consists of a code for generating a surface triangulation, and a code for discretization of the computational domain using tetrahedral elements. The surface triangulation code employs the advancing front technique, and the volume discretization code employs the Delaunay approach. FELISA software has two sets of flow solvers—one applicable for transonic flows and the other for hypersonic flows. The hypersonic flow solver has options for perfect gas air, equilibrium air, equilibrium Mars gas (0.97 CO_2 and 0.03 N_2, by mass), CF_4 gas, CO_2 gas, and a finite rate Mars gas. The equilibrium Mars gas option was added for the present study. The hypersonic flow solver with the equilibrium Mars gas option was used in the present study. FELISA software also includes several post-processing codes, including the one to compute the aerodynamic coefficients by integrating the surface pressures. More information on FELISA may be found in reference [1].

Geometry

The baseline '07 Mars lander aeroshell has a 3.75 m. diameter blunt conical forebody with a 70-deg. half-cone angle. The nose radius is 0.9124 m. and the shoulder radius is 0.0914 m. Figure 1 shows the geometrical shape of the baseline aeroshell. The reference quantities used to non-dimensionalize the aerodynamic loads

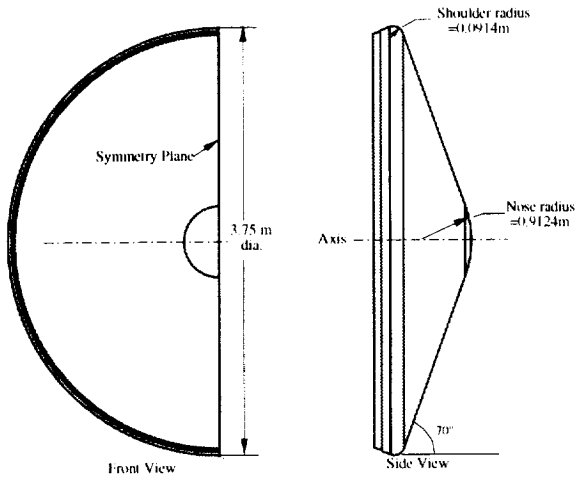

Figure 1: The basic geometry of '07 Mars lander aeroshell

are as follows:

Reference area, S_{ref}:	11.045 sq.m.
Reference length for pitching moment, l_{ref}:	3.75 m.
Pitching moment reference point:	on the axis, 0.8018 m. behind the nose.

This baseline shape being symmetric would trim at $\alpha = 0$ degrees with an L/D value of 0.0. In order to get the required L/D of -0.25 at the trim angle of attack, several modifications were made to the shape of the vehicle. These modifications were in the form of tabs and bumps of different shapes and sizes. Figures 2 - 6 show the configurations considered in the present study. They include flaps shown in Fig. 2, tabs (aft and forward) shown in Fig. 3, bumps of three different shapes shown in Fig. 4, flush flap as shown in Fig. 5, and canted flaps (80°and 90°) shown in Fig. 6.

Grids

All the configurations studied here are symmetric and the freestream flow is also symmetric. Hence only one half of the body is simulated in these computations. The geometrical information of these configurations was available in the form of IGES files. These IGES files were processed using the GridTool [5] software. The computational domains were chosen to be sufficiently large with the surfaces of the bounding box sufficiently away from the body so that, except for the exit plane, all the boundary surfaces were in the freestream flow. The computational domains were made small enough so that the volume within these domains that were not influenced by the body was small. Figure 7 shows the computational domain used the configuration "Wide Flap 90". This is typical of all the computational domains used. The minimum grid spacing was 0.80 cm, and was chosen such that there were 10–15 points between the body and the bow shock in front of the body. This provided sufficient resolution of flow features in that region. Choosing the appropriate computational domain and specifying the grid spacings was done using GridTool. Finally, a set of FELISA data files required by the FELISA grid generator were created.

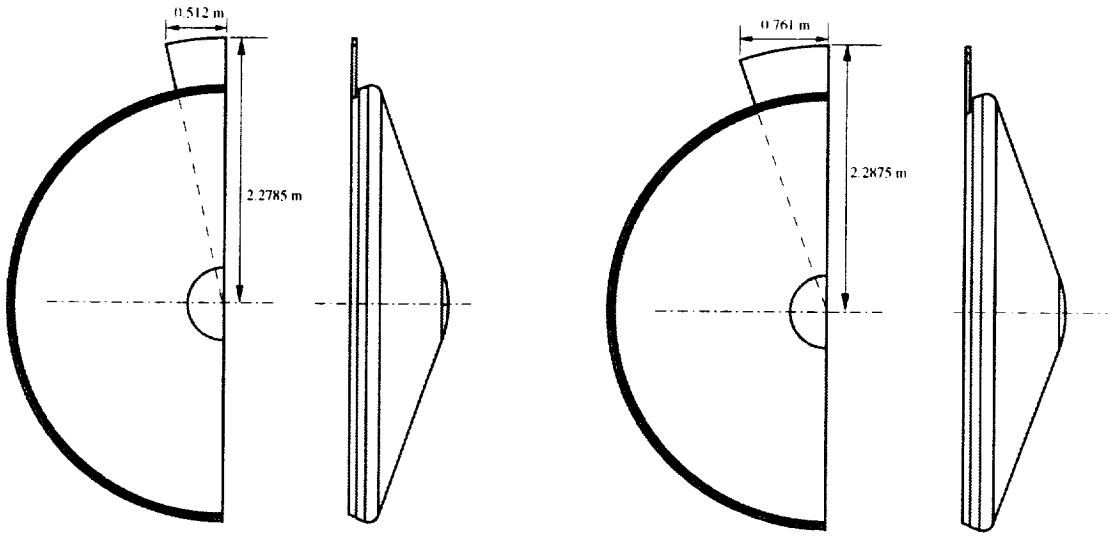

(a) Big Flap

(b) Large Tab

Figure 2: Configurations with a "flap"in the aft position considered in the present study

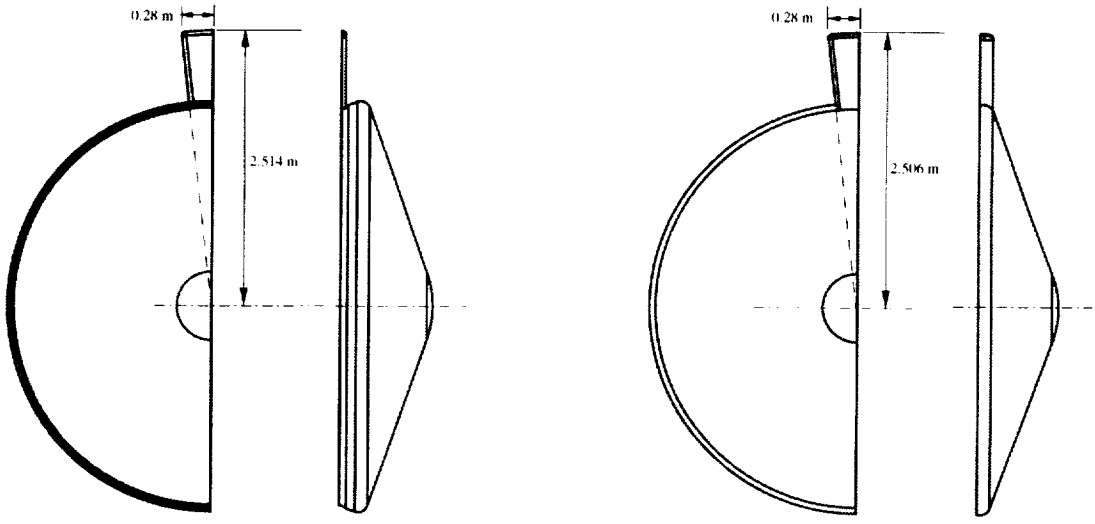

(a) Aft_tab

(b) Forward tab

Figure 3: Configurations with a "tab" considered in the present study

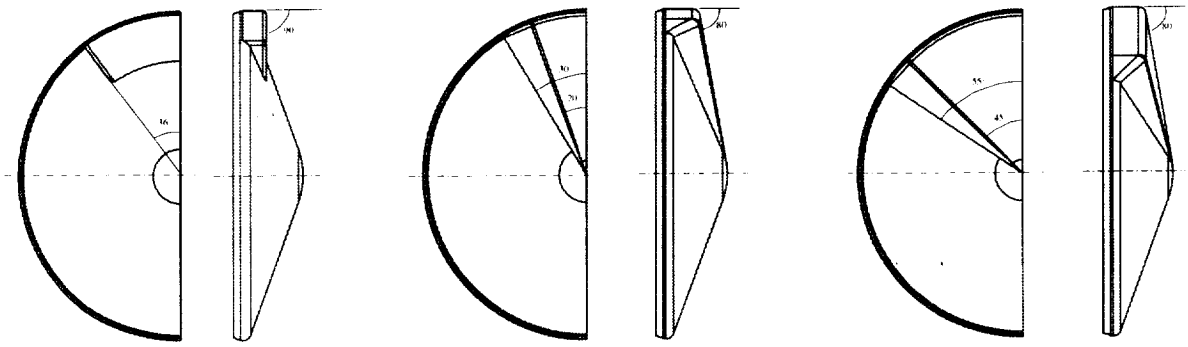

(a) Big Bump (b) Dual Cone 70-80-40 (c) Dual Cone 70-80-90

Figure 4: Configurations with a "bump" considered in the present study

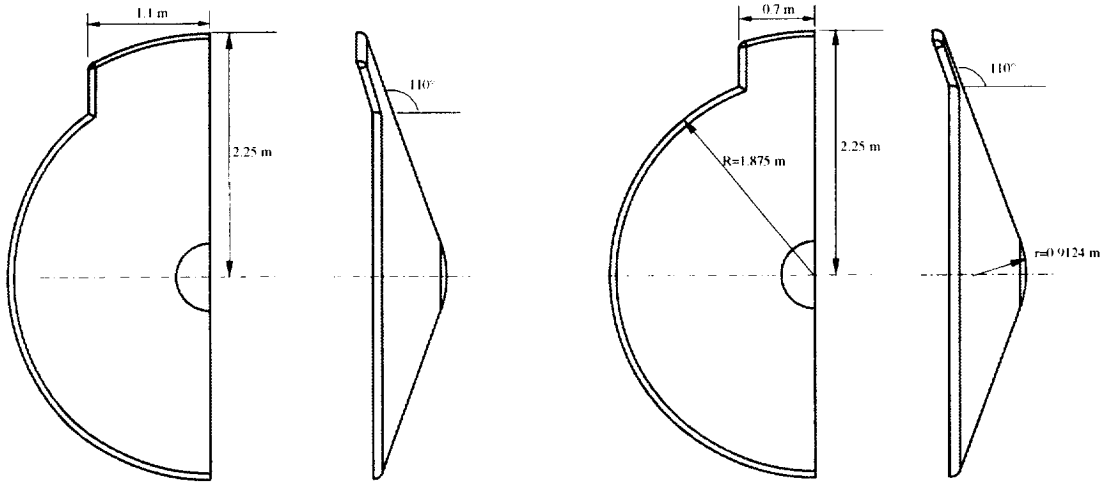

(a) Wide-Flap 70 (WF-2.2-2.25-70) (b) Wide-Flap 70N (WF-2.2-2.25-70_narrow)

Figure 5: Configurations with flush "wide flap" considered in the present study

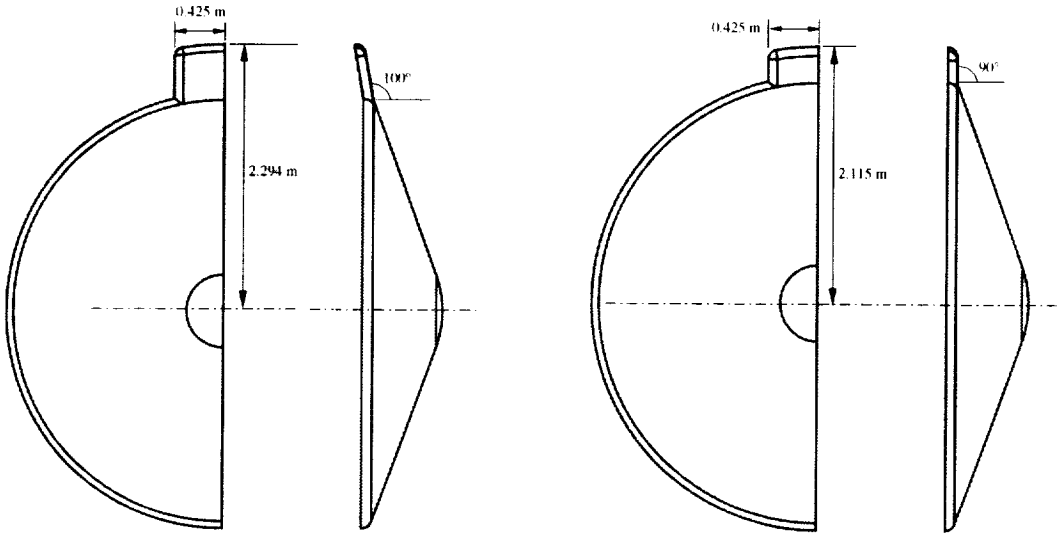

(a) Wide-Flap 80 (WF-.8-.5-80)

(b) Wide-Flap 90 (WF-.8-.3-90)

Figure 6: Configurations with canted "wide flap" considered in the present study

Using the data files and the FELISA surface triangulator, the surface triangulation was generated. The body surface triangulation (near the tab) and the triangulation of the symmetry plane for the "Wide Flap 90" case are shown in fig. 8. This grid has 55,214 surface points on the entire body, and 19,731 points on the symmetry plane. After the surface triangulation was done, the volume grid of tetrahedral elements was generated for each case. The tetrahedral (volume) grid for this case (not shown) has over 1.6M points. The processing of the IGES files and grid generation was done on an SGI Onyx computer with 2GB memory. Generation of surface triangulation generally took 20–30 minutes and the volume grid generation required 3–4 hours on an SGI Octane computer.

Flow Solution

The unstructured grids were partitioned so that the solutions could be run on a parallel computer using (typically) 16–32 processors. The FELISA hypersonic flow solver with the Mars gas option was used for all the flow computations. Each flow solution was started with the low-order option, and after a few hundred iterations, the higher-order option was turned on, and the solution was run to convergence. After every 100 iteration, the surface pressures were integrated, and the aerodynamic loads, namely the normal and the axial forces, and the pitching moment acting on the body were computed. The flow solution was assumed to be converged when these integrated loads remained essentially constant. This required 8000–10000 iterations, and 180 200 hours of CPU time. Aerodynamic loads obtained by integrating the surface pressures were non-dimensionalized in the conventional manner, and the aerodynamic coefficients namely, C_N, C_A, C_L, C_D, C_m, and L/D were obtained.

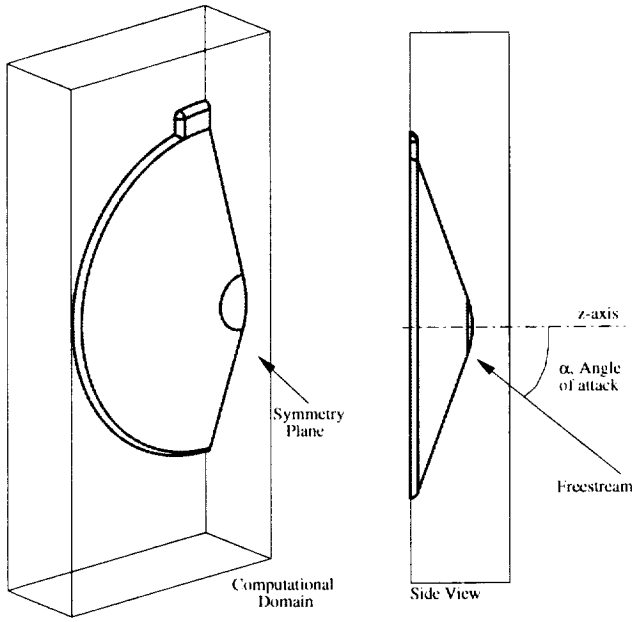

Figure 7: Computational domain for the "Wide-Flap 90" configuration

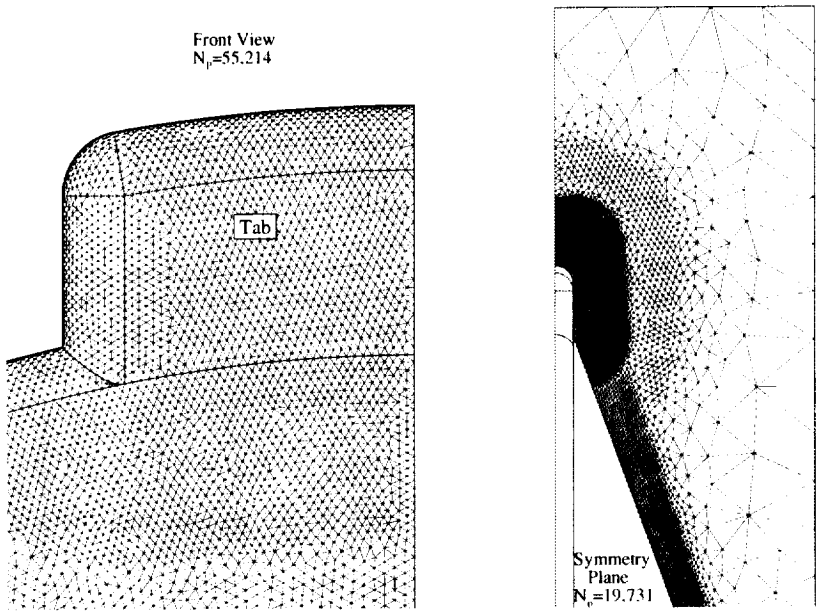

Figure 8: Surface grids for the "Wide-Flap 90" configuration

All the computations reported here were done for a freestream Mach number of 23.7 and for 10, 15, and 20 degrees angles of attack. Note that the trim devices are on the lee side of the aeroshell at positive angles of attack as shown in Fig. 7. The freestream gas was assumed to Mars atmospheric gas in chemical equilibrium. The freestream velocity, density, temperature, and Mach number correspond to those at the peak heating point on a preliminary '07 Mars lander trajectory, and are shown below:

Velocity, V_∞:	4920 m/s
Density, ρ_∞:	4.15 10^{-4} (kg/m^3)
Temperature, T_∞:	158.5 $Kelvin$
Mach Number, M_∞:	23.7
Mars Atmosphere:	0.97 CO_2 and 0.03 N_2, (by mass)

Results and Discussion

The results of the present computations are listed in Tables 1, 2, and 3. It should be recalled at this point that the present computations are inviscid; hence the skin friction and flow separation effects are absent. In the present case, the axial force coefficients are large due to the very high pressures on the blunt forebody. Absence of the skin friction in inviscid computations leads to somewhat lower axial forces. But contribution of the skin friction to axial force in the present case is expected to be a small fraction of the total axial force. Further, since the boundary layer is absent, the effects of boundary layer separation (over the forebody) on the aerodynamic loads are also absent. This could become a factor in those cases where there is a possibility of flow separation on the forebody, like the canted flaps configurations. In viscous flow, the flow over the body approaching the canted flaps could separate due to the adverse pressure gradients.

In the present computations, only the forebody is simulated and the aftbody is ignored. Hence the aftbody contributions to the aerodynamic loads are absent in the present results. The present flow solver could not simulate the flow over the aftbody where the flow is separated and highly viscous dominated. At low Mach number conditions, the pressure in the separated flow regions over the aftbody would be large, and contribute significantly to the axial force See, for example, Gnoffo, et al. [6]. However, at Mach 23.7, the pressures on the aft-body are going to be very small, and contribute very little to the aerodynamic characteristics of the vehicle.

The present results are sorted into three groups for convenience. The first group is called the "TABS" group, and consists of the Big flap, the Large tab, the Aft-tab, and the Fwd-tab. The second group is called the "BUMPS" and consists of the BigBump, the DualCone 70-80-40, and the DualCone 70-80-90. The third group is called the "FLAPS", and consists of the Wide Flap 70 (WF70), the Wide Flap 70N (WF70N), the Wide Flap 80 (WF80), and the Wide Flap 90 (WF90) configurations.

The "TABS" configurations:

As noted before, the TABS group included the Big flap, the Large tab, the Aft-tab, and the Fwd-tab configurations. The C_p contours (for α=15 degrees) on the symmetry plane in the vicinity of the flap for each of the four cases are shown in Fig. 9. In all these cases, there is a strong shock from the flap. This shock is formed as the flow is turned due the flap, and can be seen in all the four cases. This shock intersects the bow shock in front of the body, and forms a complex shock interference pattern. Depending on the size of the flap and its location relative to the bow shock, the flow from the shock intersection could impinge on the

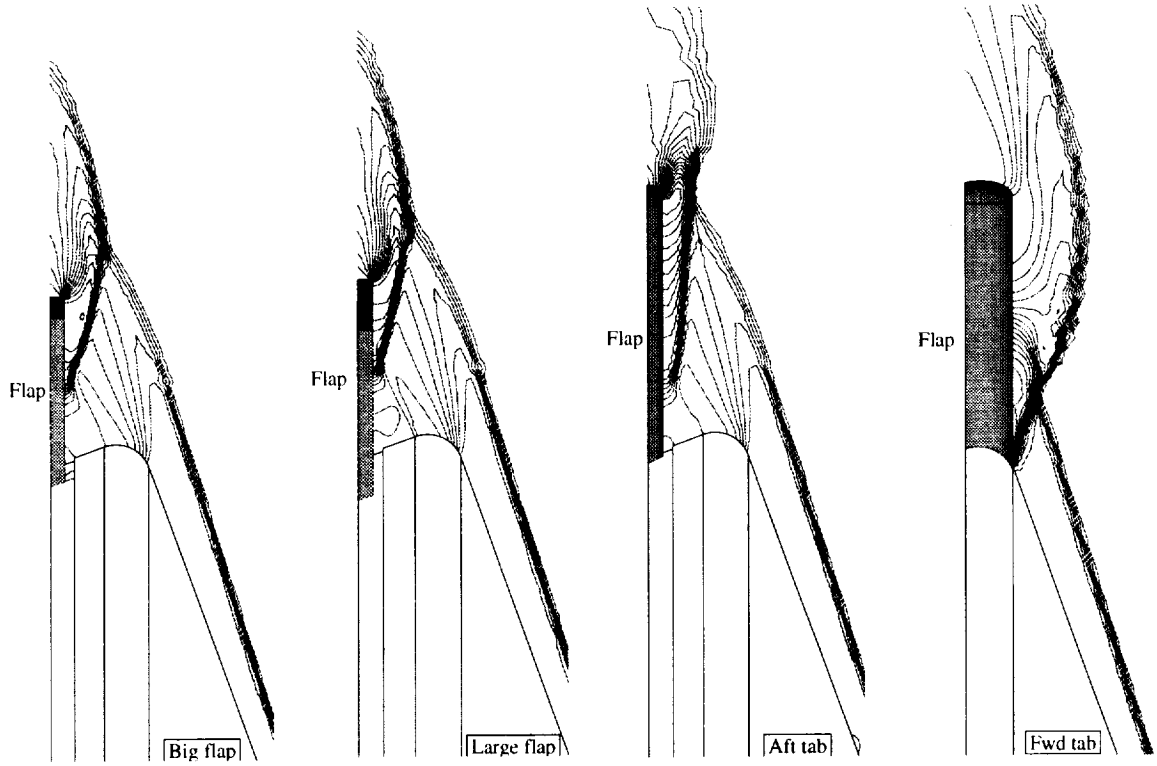

Figure 9: C_p contours on the symmetry plane near the flap for the "TAB" configurations, α=15 degrees

flap. This happens for the fwd-tab configuration, see Fig. 9. Such an impingement would lead to high surface pressures. For the first three configurations where the flap in set back from the maximum body diameter location, the interference flow does not affect the flap. For the Big Flap and the Large tab configurations, the maximum values of surface C_p, which occur at 20 degrees angle of attack are 2.81 and 2.87, respectively. For the Aft-tab configuration, the flow from the shock intersection grazes the flap tip. This leads to slightly higher C_p values (3.76). But for the Fwd-tab configuration, the flow from the shock interference impinges on the flap. The peak values of the C_p in this case is 4.20. The surface C_p contours plot for the Large tab case is shown in Figure 10. The high pressures on the flap produce a large axial force, and, because of the location of the flap, produce a large pitching moment. The large pressure gradients associated with such locally high pressures will lead also to high surface heating.

As noted before, the Big flap, the Large tab, the Aft-tab have the tabs located aft of the maximum diameter position. As a result, these configurations have some space between the shoulder and the flaps, where a "re-circulatory" flow is observed. (This re-circulatory flow in the present inviscid computations is surprising, and is possibly due to artificial viscosity in the numerical scheme used in the flow solver.) This is shown in Figure 11 for the Large tab configuration. Similar features are observed also for the Aft-tab and the Large tab configurations. In actual viscous flows, such a flow could lead to high surface heating and is considered undesirable. For the fwd-tab configuration, such a flow re-circulatory flow does not exist.

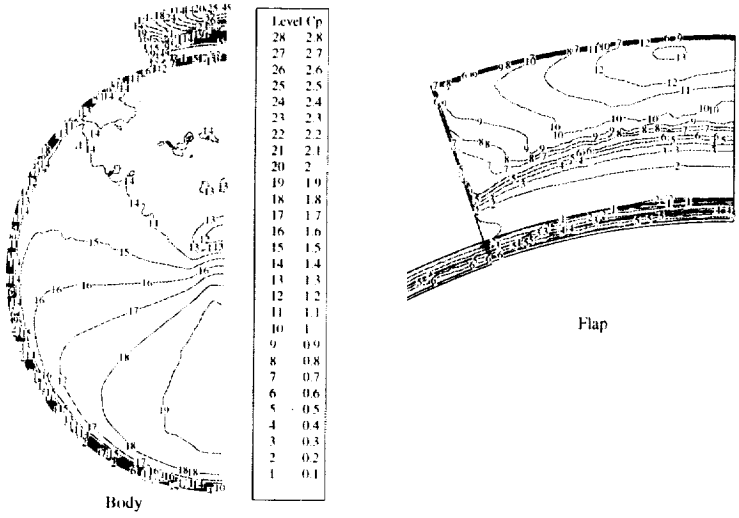

Figure 10: C_P contours on the body for the Large tab configuration, α=15 degrees

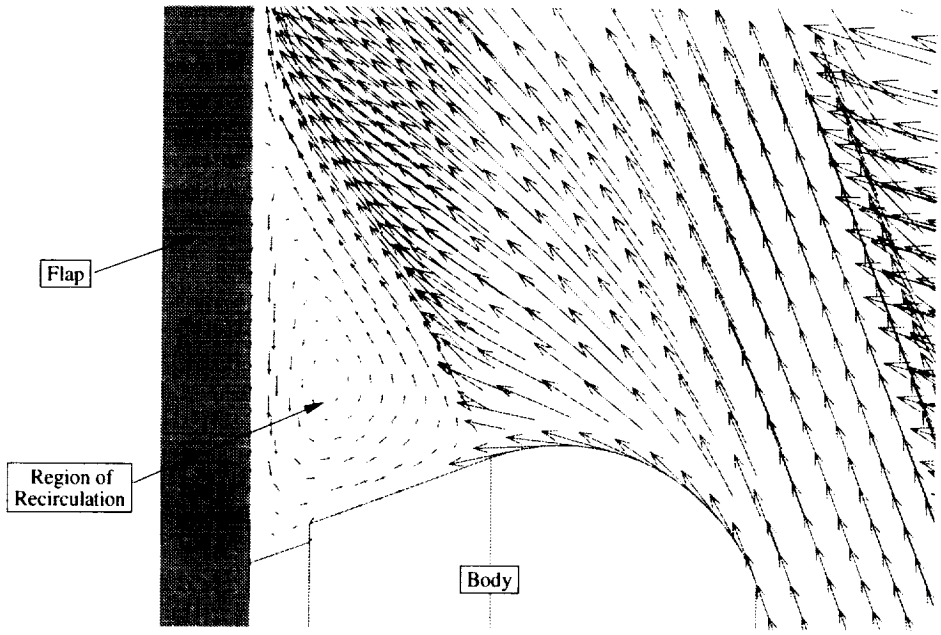

Figure 11: Recirculatory flow for the Large tab configuration, α=15 degrees

α (*deg.*)	C_N	C_A	C_m	C_L	C_D	L/D
Configuration: No Tab (Base line)						
10	3.2923E-02	1.6249	-2.0272E-02	-2.4974E-01	1.6059	-1.5551E-01
15	5.4037E-02	1.5324	-3.4823E-02	-3.4441E-01	1.4941	-2.3051E-01
20	7.6512E-02	1.4266	-5.0406E-02	-4.1602E-01	1.3667	-3.0440E-01
Configuration: Big flap						
10	2.8492E-02	1.6867	1.4809E-02	-2.6483E-01	1.6660	-1.5896E-01
15	5.1645E-02	1.5868	-3.9316E-03	-3.6081E-01	1.5461	-2.3337E-01
20	7.4887E-02	1.4734	-2.3914E-02	-4.3356E-01	1.4102	-3.0746E-01
Configuration: Large tab						
10	2.2152E-02	1.7155	3.0338E-02	-2.7608E-01	1.6933	-1.6304E-01
15	4.8900E-02	1.6166	1.2206E-02	-3.7118E-01	1.5742	-2.3579E-01
20	7.2412E-02	1.4974	-1.0772E-02	-4.4409E-01	1.4319	-3.1015E-01
Configuration: Aft-tab (solid-aft)						
10	2.9782E-02	1.6812	1.4381E-02	-2.6260E-01	1.6608	-1.5812E-01
15	5.1312E-02	1.5872	-1.2232E-03	-3.6124E-01	1.5464	-2.3360E-01
20	7.4273E-02	1.4747	-2.0810E-02	-4.3459E-01	1.4112	-3.0796E-01
Configuration: Fwd-tab (solid-fwd)						
10	3.2493E-02	1.6806	9.2573E-03	-2.5983E-01	1.6607	-1.5646E-01
15	5.3200E-02	1.5939	-2.2004E-03	-3.6113E-01	1.5533	-2.3249E-01
20	7.4714E-02	1.4932	-1.5242E-02	-4.4050E-01	1.4287	-3.0832E-01

Table 1: Aerodynamic coefficients for "TABS" configuration with equilibrium Mars gas, Mach 23.7

However, the flow on the body approaching the flap could separate due the adverse pressure gradient at the junction of the flap and the body.

The computed aerodynamic data for these configurations are presented in Table 1, and shown plotted in Figures 12 to 14. The pitching moment curves, Fig. 12, show that the trim angle of attack is 17.7 degrees for the Large tab configuration, and is 14.5 degrees for the other configurations. An examination of Fig. 13 shows that "TABS" configurations have very similar L/D characteristics. The trim L/D for the Large tab configuration is -0.275, and for the other configurations in this group is about -0.225. Thus it is observed that proper selection of the flap size could lead to the desired L/D of -0.25 at the trim condition. Figure 14 shows the C_D for the four configurations.

The "BUMPS" configurations:

The second group called the "BUMPS" consist of the BigBump, the DualCone 70-80-40, and the DualCone 70-80-90 configuration. The computed aerodynamic data for these configurations are presented in Table 2, and shown plotted in Figures 18 to 20. The C_p contours on the body surface and on the symmetry plane

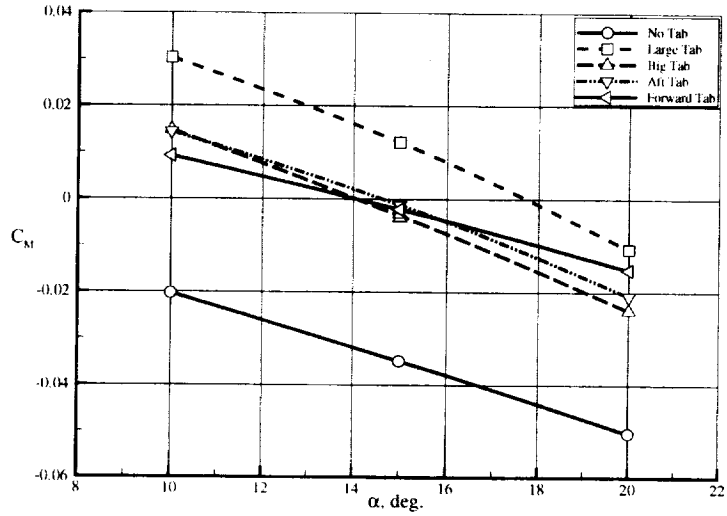

Figure 12: Pitching moment coefficient for the "TABS" configurations

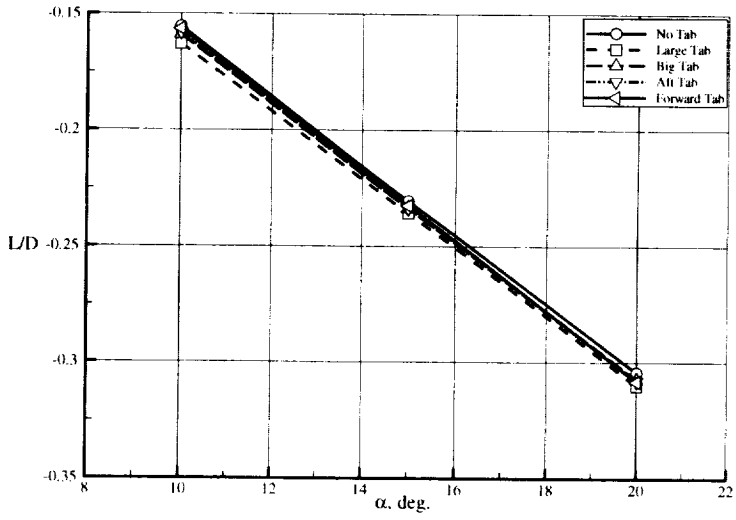

Figure 13: Lift-to-Drag ratio for the "TABS" configurations

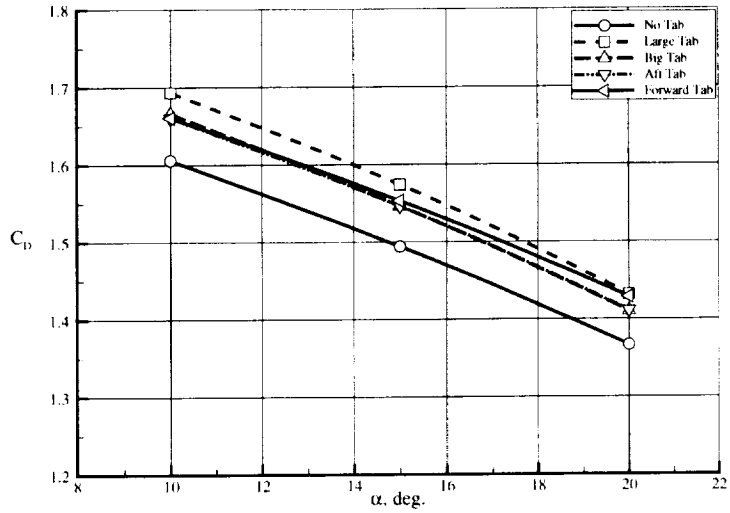

Figure 14: Drag coefficient for the "TABS" configurations

for the three configurations at α=15 degrees are shown in Figures 15 to 17. For the BigBump configuration there is a region of very high pressures (C_{pmax}=8.4) over the "bump". This high pressure is due to the shock interference as observed in the "TABS" configurations, and is considered undesirable from surface heating consideration. The C_p contours on the body surface and on the symmetry plane for the DualCone 70-80-40 and DualCone 70-80-90 configurations shown in Figs. 16 and 17 do not show any high pressure spots. The computed aerodynamic data for these configurations are presented in Table 2, and shown plotted in Figures 18 to 20. The pitching moment curves for these two cases indicated that the DualCone 70-80-40 configuration trims at an α of about 8 degrees, where is L/D is only -0.1, whereas the DualCone 70-80-90 configuration trims at 15 degrees, where the L/D is about -0.175. Hence these configurations are not suitable for the present application. Among the three configurations in this group, the BigBump has a nonlinear pitching moment variation with angle of attack. The C_m curve barely grazes the C_m =0 line, indicating the configuration hardly trims. All the configurations in the "BUMPS" group are judged to be unsuitable for the present application.

The "FLAPS" configurations:

This group called the "FLAPS" consists of the Wide Flap 70 (WF70), the Wide Flap 70N (WF70N), the Wide Flap 80 (WF80), and the Wide Flap 90 (WF90) configurations. The computed aerodynamic results for these configurations are tabulated in Table 3 and shown plotted in Figures 25 to 27.

Figure 21 shows the C_p contours on the symmetry plane for the WF70, WF80, and WF90 configurations for α =15 degrees. The WF70N is not included in this figure. The only difference between WF70 and WF70N is that the latter has a flap that is not as wide as that of the former. For both WF70 and WF70N cases, the flap is an extension of the conical part of the body. Hence, the flow approaching the flap flows over the flap smoothly. For the WF80 and WF90 configurations, however, the flow has to turn abruptly at

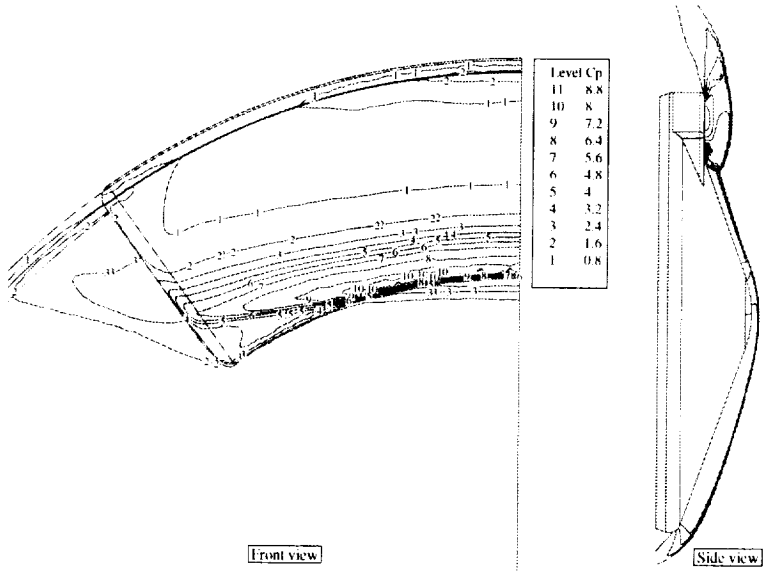

Figure 15: C_P contours for the BigBump configuration near the bump and on the symmetry plane, α=15 degrees

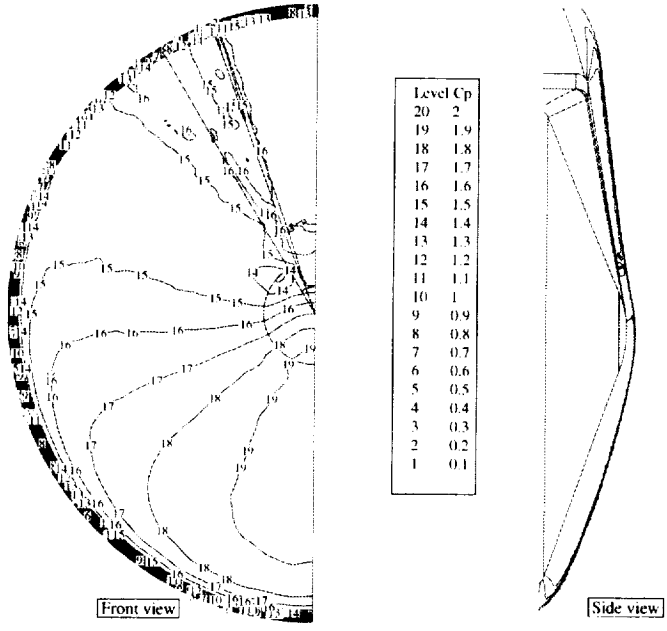

Figure 16: C_P contours for the DualCone 70-80-40 configuration on the body and on the symmetry plane, α=15 degrees

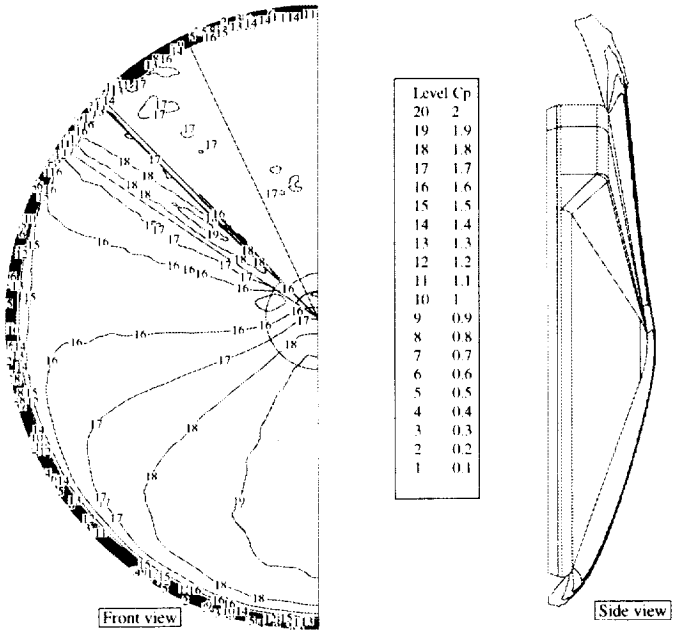

Figure 17: C_P contours for the DualCone 70-80-90 configuration on the body and on the symmetry plane, α=15 degrees

α (*deg.*)	C_N	C_A	C_m	C_L	C_D	L/D
Configuration: BigBump(R) (solid-.3-72-20)						
10	8.2426E-02	1.7278	2.0614E-02	-2.1885E-01	1.7158	-1.2755E-01
15	1.0637E-01	1.6181	-3.4294E-03	-3.1605E-01	1.5905	-1.9871E-01
20	1.2617E-01	1.5746	6.8939E-03	-4.1997E-01	1.5228	-2.7580E-01
Configuration: DualCone 70-80-40 (dualCone-70-80-40)						
10	8.9553E-02	1.6626	-5.8626E-03	-2.0052E-01	1.6529	-1.2131E-01
15	1.0350E-01	1.5838	-1.6877E-02	-3.0993E-01	1.5566	-1.9911E-01
20	1.1727E-01	1.4915	-2.9545E-02	-3.9993E-01	1.4417	-2.7741E-01
Configuration: DualCone 70-80-90 (dualCone-70-80-90)						
10	1.4072E-01	1.7151	9.6060E-03	-1.5924E-01	1.7135	-9.2935E-02
15	1.5129E-01	1.6468	2.2144E-04	-2.8010E-01	1.6299	-1.7186E-01
20	1.6093E-01	1.5624	-1.1694E-02	-3.8315E-01	1.5232	-2.5154E-01

Table 2: Aerodynamic coefficients for the "BUMPS" configuration with equilibrium Mars gas, Mach 23.7

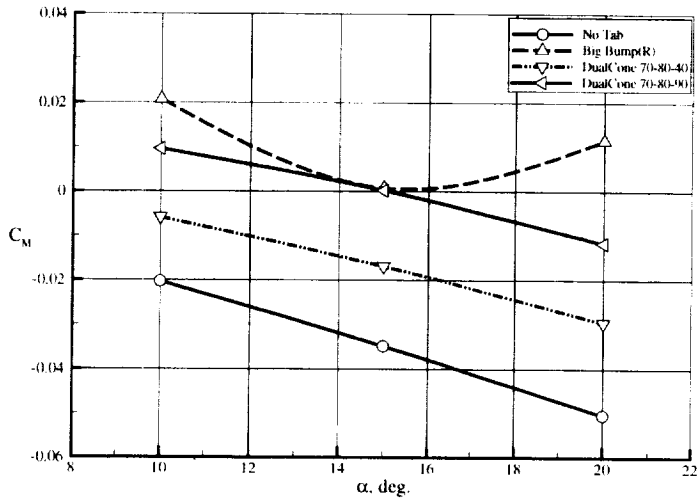

Figure 18: Pitching moment coefficient for the "BUMPS" configurations

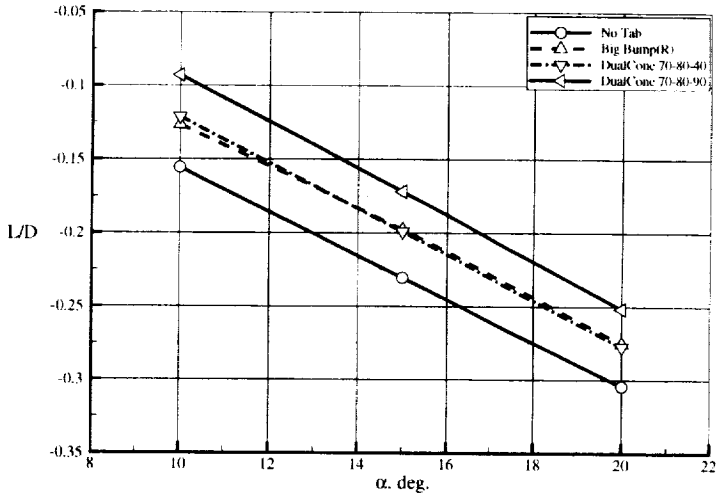

Figure 19: Lift-to-Drag ratio for the "BUMPS" configurations

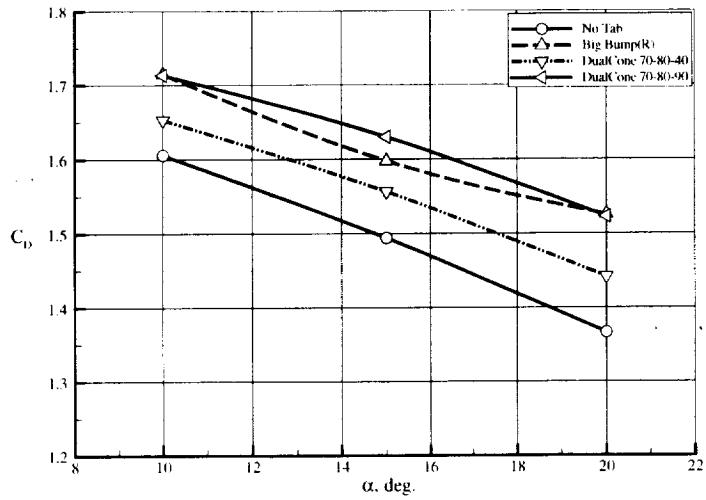

Figure 20: Drag coefficient for the "BUMPS" configurations

the junction of the body and the flap. This is particularly severe in the WF90 case where the flow has to turn through a 20 degrees angle. Because the flow approaching the flap is supersonic, and it has to change direction at the flap, an oblique shock starts from the junction of flap and the body. In viscous flows, the pressure rise associated with this shock could lead to local boundary layer separation. Since the present computations are inviscid, such a flow separation is absent. The shock due to the flap and the bow shock in front of the body interfere. For certain conditions, the interference could impinge on the flap. This happens for the WF90 configuration. This is clearly evident from Fig. 21. Such an impingement generally leads to high surface pressures.

The pressure distributions on the three flaps for α =15 degrees are shown in Figs. 22 to 24. The maximum values of C_p are 1.98 for WF70, 2.47 for WF80, and 7.37 for WF90. Due to the flow impingement, very high C_p values are observed on the WF90. High pressures on the flap would lead to larger axis force due to the flap, and because of its moment arm produce large pitching moment. In the present case such a comparison cannot be made because the areas of the flaps in the three cases are different. It should be borne in mind is that large pressure gradients are generally associated with locally high heating which is not desirable.

The pitching moment coefficients and the lift-to-drag values are shown plotted in Fig. 25 and 26. All the configuration in this group have stable pitching moment characteristics. The WF70 configuration has a trim angle of attack of 18.8 degrees, and a corresponding L/D of -0.33. The WF70N has a trim angle of only 14 degrees, and a trim L/D of -0.26. The WF80 and WF90 configurations exhibit a slightly nonlinear C_m characteristics. This is particularly evident for the WF90 case. Further, the trim L/D values for these two cases are about -0.25. Thus, all the "FLAPS" configurations can meet the required L/D of -0.25 at the trim conditions. Proper sizing of the flaps can tailor the L/D. Figure 27 shows the variation of the C_D for the four configurations.

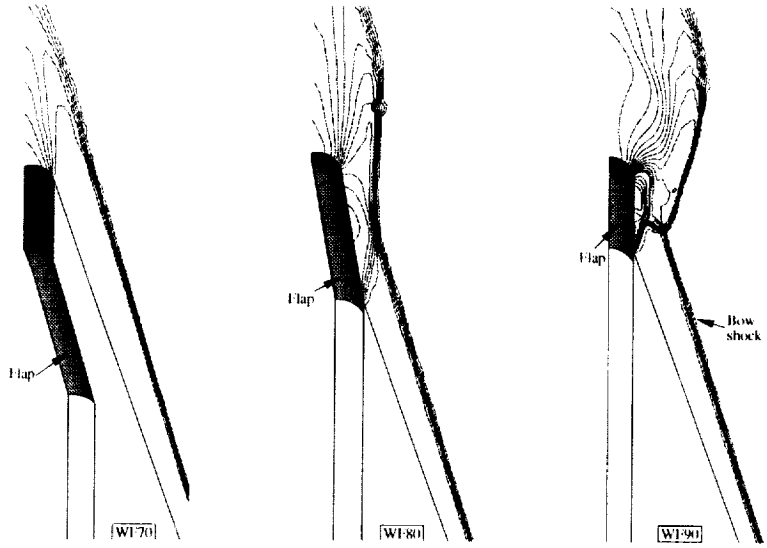

Figure 21: Symmetry plane C_p contours for the WF70, WF80, and WF90 configurations for α=15 degrees

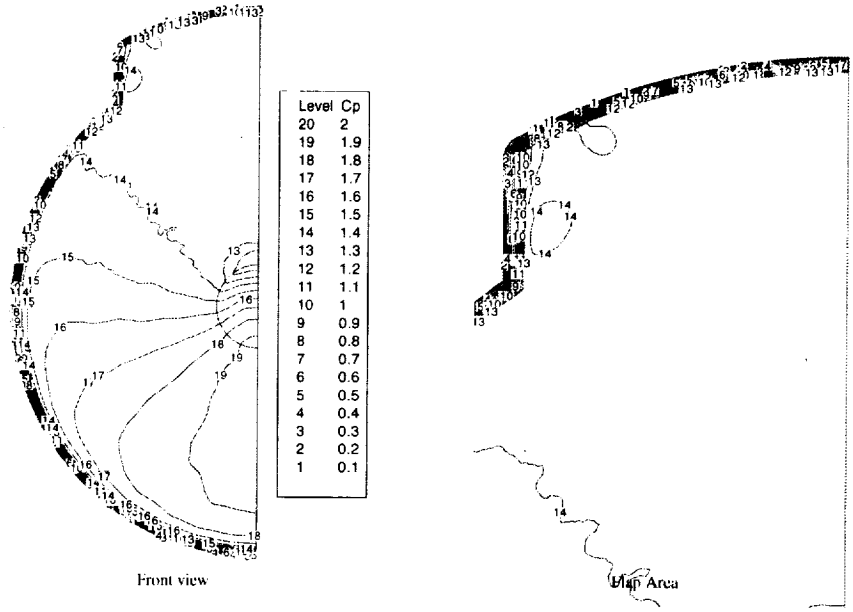

Figure 22: C_p contours for the WF70 configuration α=15 degrees

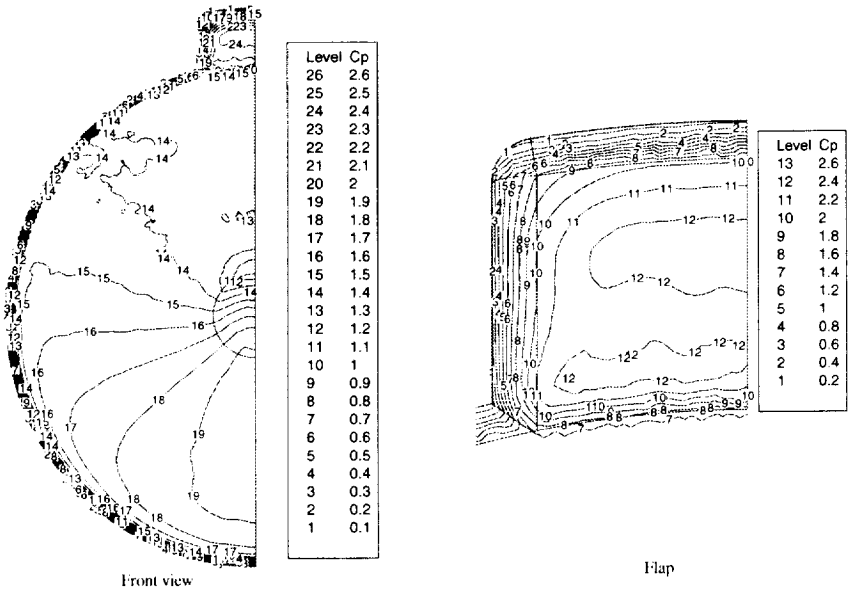

Figure 23: C_p contours for the WF80 configuration α=15 degrees

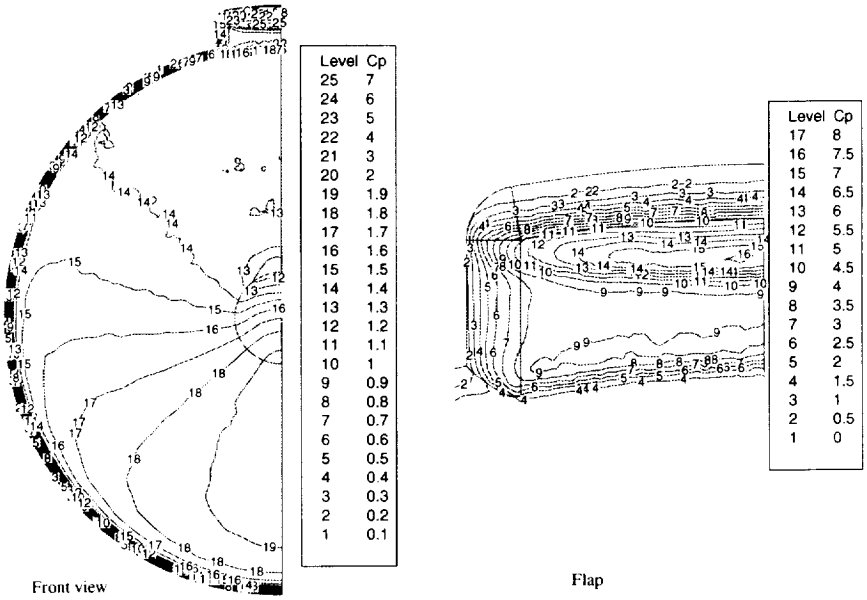

Figure 24: C_p contours for the WF90 configuration α=15 degrees

α (*deg.*)	C_N	C_A	C_m	C_L	C_D	L/D
Configuration: Wide Flap 70 (WF-2.2-2.25-70)						
10	-8.1397E-03	1.7421	3.7963E-02	-3.1053E-01	1.7142	-1.8115E-01
15	1.6088E-02	1.6375	1.6900E-02	-4.0828E-01	1.5859	-2.5745E-01
20	4.2235E-02	1.5162	-6.1653E-03	-4.7888E-01	1.4392	-3.3274E-01
Configuration: Wide Flap 70N (WF-2.2-2.25-70_narrowflap)						
10	7.2172E-03	1.6953	1.5520E-02	-2.8728E-01	1.6708	-1.7194E-01
15	2.9871E-02	1.5954	-3.1296E-03	-3.8406E-01	1.5487	-2.4798E-01
20	5.4471E-02	1.4794	-2.3776E-02	-4.5481E-01	1.4088	-3.2283E-01
Configuration: Wide Flap 80 (WF-.8-.5-80)						
10	1.9338E-02	1.6983	1.6264E-02	-2.7586E-01	1.6758	-1.6461E-01
15	3.9086E-02	1.6053	1.5700E-03	-3.7772E-01	1.5607	-2.4202E-01
20	6.0396E-02	1.4972	-1.5445E-02	-4.5531E-01	1.4275	-3.1895E-01
Configuration: Wide Flap 90(R) (WF-.8-.3-90)						
10	3.2508E-02	1.6949	1.3960E-02	-2.6230E-01	1.6748	-1.5662E-01
15	5.0208E-02	1.6118	4.7854E-03	-3.6867E-01	1.5699	-2.3484E-01
20	7.0650E-02	1.4935	-1.7627E-02	-4.4442E-01	1.4276	-3.1131E-01

Table 3: Aerodynamic coefficients for the "FLAPS" configurations with Mars gas in equilibrium, Mach 23.7

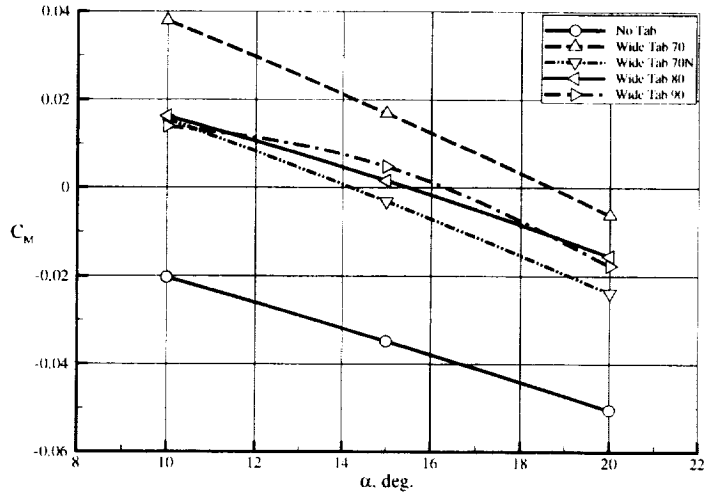

Figure 25: Pitching moment coefficient for the "FLAPS" configurations

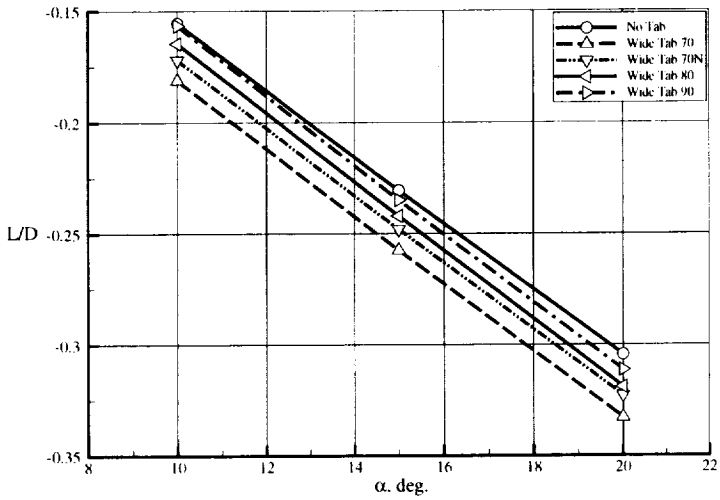

Figure 26: Lift-to-Drag ratio for the "FLAPS" configurations

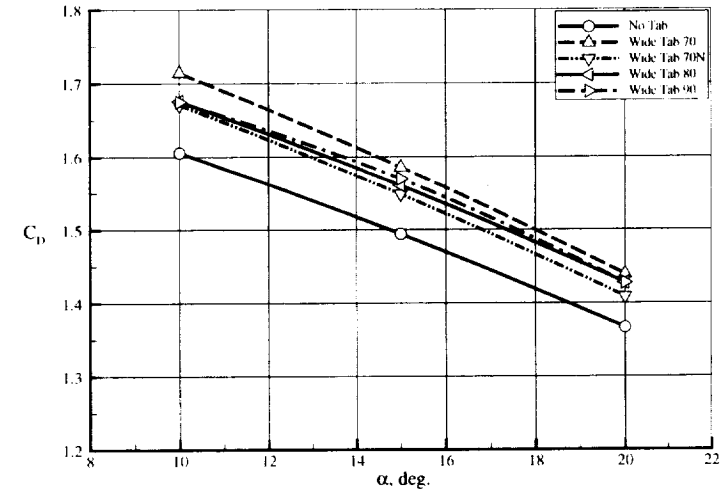

Figure 27: Drag coefficient for the "FLAPS" configurations

Conclusions

A computational study was done on several aeroshell configuration for a proposed '07 Mars lander to assist in the selection of a suitable configuration with the desired aerodynamic characteristics. The inviscid longitudinal aerodynamic characteristics for 11 different configurations were computed in Mars gas environment at Mach 23.7 with the freestream conditions corresponding to the peak heating point on an initial trajectory at three angles of attack namely 10, 15, and 20 degrees. The FELISA software was used for all these computations. The pitching moment and lift-to-drag ratios of each of the configurations were examined for stable pitching moment characteristics and desired lift-to-drag ratio at the trim angle of attack. Based on the findings of the present study, two new configurations for flaps of 70 degrees and 80 degrees were selected for further study. Detailed flow solutions were done for these two configurations over a Mach number range of 2 23.7 at 10, 15, and, 20 degrees angles of attack as presented in Ref. [7].

Acknowledgments

The author wishes to express his gratitude to Dr. K. Sutton of the Aerothermodynamics Branch (AB), NASA Langley Research Center for many helpful discussions during the course of this work. The work described herein was performed at Lockheed Martin Engineering & Sciences in Hampton, Virginia, and was supported by the AB, NASA Langley under the contract NAS1-96014. The technical monitor was Mr. K.J. Weilmuenster.

References

[1] Peiro, J., Peraire, J., and Morgan, K., "FELISA System Reference Manual and User's Guide," Tech. Report, University College of Swansea, Swansea, U.K., 1993.

[2] Frink, N.T., Pirzadeh, S., and Parikh, P., "An Unstructured-Grid Software System for Solving Complex Aerodynamic Problems," NASA CP-3291, pp. 289-308, May 9-11, 1995.

[3] Prabhu, R.K., "An Inviscid Computational Study of an X-33 Configuration at Hypersonic Speeds," NASA CR-1999-209366, July 1999.

[4] Prabhu, R.K., "Computational Study of a McDonnell Douglas Single-Stage-to-Orbit Vehicle Concept for Aerodynamic Analysis," NASA CR 20160, September 1996.

[5] Samereh, J., "GridTool: A Surface Modeling and Grid Generation Tool," NASA CP 3291, May 1995.

[6] P.A. Gnoffo, K.J. Weilmuenster, R.D. Braun, and C.I. Cruz., "Influence of Sonic-Line Location on Mars Pathfinder Probe Aerothermodynamic," *Journal of Spacecraft and Rockets*, Vol. 33, No. 2, March-April 1996.

[7] Prabhu, R. K., "Inviscid Flow Computaions of Two '07 Mars Lander Aeroshell Configurations over a Mach Number Range of 2 to 24," NASA CR-2001-210852, April 2001.

REPORT DOCUMENTATION PAGE

Form Approved
OMB No. 0704–0188

1. AGENCY USE ONLY *(Leave blank)*	2. REPORT DATE	3. REPORT TYPE AND DATES COVERED
	April 2001	Contractor Report

4. TITLE AND SUBTITLE
Inviscid Flow Computations of Several Aeroshell Configurations for a '07 Mars Lander

5. FUNDING NUMBERS
C NAS1-96014
WU 242-80-01-01

6. AUTHOR(S)
Ramadas K. Prabhu

7. PERFORMING ORGANIZATION NAME(S) AND ADDRESS(ES)
Lockheed Martin Engineering & Sciences Company
C/O NASA Langley Research Center
Hampton, VA 23681–2199

8. PERFORMING ORGANIZATION REPORT NUMBER

9. SPONSORING/MONITORING AGENCY NAME(S) AND ADDRESS(ES)
NASA Langley Research Center
Hampton, VA 23681–2199

10. SPONSORING/MONITORING AGENCY REPORT NUMBER
NASA/CR–2001–210851

11. SUPPLEMENTARY NOTES
Langley Technical Monitor: K. James Weilmuenster

12a. DISTRIBUTION/AVAILABILITY STATEMENT
Unclassified-Unlimited
Subject Category 02
Distribution: Nonstandard
Availability: NASA CASI (301) 621–0390

12b. DISTRIBUTION CODE

13. ABSTRACT ***(Maximum 200 words)***

This report documents the results of an inviscid computational study conducted on several candidate aeroshell configurations for a proposed '07 Mars lander. Eleven different configurations were considered, and the aerodynamic characteristics of each of these were computed for a Mach number of 23.7 at 10, 15, and 20 degrees angles of attack. The unstructured grid software FELISA with the equilibrium Mars gas option was used for these computations. The pitching moment characteristics and the lift-to-drag ratios at trim angle of attack of each of these configurations were examined to make a selection. The criterion for selection was that the configuration should be longitudinally stable, and should trim at an angle of attack where the L/D is -0.25. Based on the present study, two configuration were selected for further study.

14. SUBJECT TERMS
Unstructured Grid CFD, Hypersonic Speeds, Mars Gas, Aerodynamic Loads

15. NUMBER OF PAGES
27

16. PRICE CODE
A03

17. SECURITY CLASSIFICATION OF REPORT	18. SECURITY CLASSIFICATION OF THIS PAGE	19. SECURITY CLASSIFICATION OF ABSTRACT	20. LIMITATION OF ABSTRACT
Unclassified	Unclassified	Unclassified	UL